Proceeding of the IEEE
International Conference on Robotics and Biomimetics
Dali, China, December 2019

Controller Design of Deployment Process for Large Deployable Reflectors*

Shaolin Lu, Xiaozhi Qi, Yucheng He & Ying Hu
Shenzhen Key Laboratory of Minimally Invasive Surgical Robotics and System,
Shenzhen Institutes of Advanced Technology, Chinese Academy of Sciences
Shenzhen, Guangdong Province, China
{sl.lu, xz.qi, yc.he & ying.hu}@siat.ac.cn

Tao Qin
Hubei University of Arts and Sciences
Xiangyang, Hubei Province, China
heu_qt@163.com

Bing Li
Harbin Institute of Technology at Shenzhen
Shenzhen, Guangdong Province, China
libing.sgs@hit.edu.cn

Jianwei Zhang
University of Hamburg
Hamburg, 22527, Germany
zhang@informatik.uni-hamburg.de

***Abstract* - Large deployable reflectors are the key technical equipment to meet the needs of geostationary mobile communication in high rail and earth observation. After being sent to the working track by the spacecraft, the space antenna is driven by a reliable and stable controller to provide a frame for forming a high-precision metal reflecting surface. This paper aims to study the optimal deployment process control strategy and method based on the deployable trajectory for a large deployable antenna. In this paper, the Backstepping controller and fuzzy PID controller are designed respectively based on the model and non-model perspectives. The feasibility of the controller is verified by simulation, and the advantages and applications of the controller are illustrated by comparison. The article lays a good foundation for the technical improvement of the antenna system.**

Index Terms – Large deployable reflectors, controller design, nonlinear system, backstepping control, fuzzy-PID control.

I. INTRODUCTION

Large deployable reflectors (LDRs) play a vital role in many space tasks, such as the modern and future satellite communications, and space exploration [1]. The application of LDR enlarges the width, distance and information capacity of satellite communication, especially in the military field, which has received great attention from various countries. Limited by the capacity of the transmitter, the antenna is typically designed to be deployable. LDRs are a type of large-scale aerospace structure that can be folded and deployed. That is, during the transportation and launch phases of the rocket, the antenna structures can be folded together to maintain a small size. After the spacecraft successfully entered space, the antenna mechanism was deployed into a large aerospace structure achieved through a series of control measures to provide a solid support frame for the metal reflecting surface, as shown in Fig. 1.

Many countries have successfully applied antennas to space missions [2], but there are numerous antenna deployments that are failure cases [3]. Therefore, the antenna deployment process is still a hot issue that needs further study. The deployable process of the antenna is a complex rigid-flexible coupling process involving the deployment of a rigid ring truss and the deployment of a flexible cable net system, which is full of uncertainties. The large-scale deployable antenna structure must be able to be deployed reliably and smoothly in the orbit, and the attitude of the spacecraft body cannot be unstable due to the impact vibration [4]. The deployment process of LDR often determines the "success and failure" of the entire space mission.

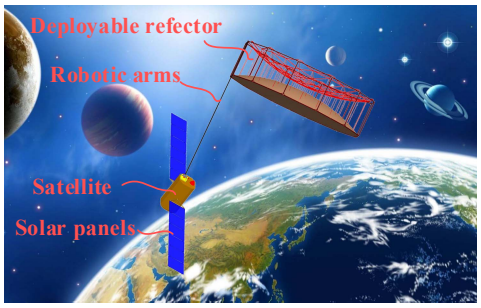

Fig. 1 Spacecraft system

The author's research team has been working on LDR related technologies for many years, and the group has achieved fruitful results in mechanism theory and design [5][6], mobility analysis [7], and development process dynamics analysis [8]. The controlled object in this paper is a large space deployable antenna researched by the team recently [9], as shown in Fig. 2. Our team is working on relevant research to complete the entire system of the new ring deployable antenna, including configuration design, dynamics analysis, profile design and surface accuracy adjustment, and the design of the expansion controller to be studied in this paper.

Some scholars have done relevant research on the development process control method of many antennas. Zhang [10][11] et al. established a multi-body system dynamics

* Corresponding authors are Xiaozhi Qi and Yucheng He. This work is partially supported by National Natural Science Foundation of China Grant #51705512 and Shenzhen Fundamental Research Funds Grant #JCYJ20170413104438332 to X. Qi, partially supported by National Natural Science Foundation of China Grant #U1613201 to B. Li, partially supported by Shenzhen Fundamental Research Funds Grant #JCYJ20160608153218487 and Shenzhen Key Laboratory Project Grant #ZDSYS201707271637577 to Y. He and Y. Hu, partially supported by Hubei Provincial Natural Science Foundation Grant #2018CFB313 to T. Qin, partially supported by the German Science Foundation and National Science Foundation of China in project Crossmodal Learning under contract Sonderforschungsbereich Transregio 169 to J. Zhang.

978-1-7281-6321-5/19//$31.00 ©2019 IEEE

equation of the deployable antenna based on the Lagrange method. A filter was designed to divide the displacement feedback signal of the system into two parts: rigid displacement and flexible vibration. Rigid and flexible controllers are designed for each of these two parts, in which the rigid controller ensures that the antenna system can move according to a pre-designed trajectory, and the flexible controller is used to suppress flexible vibration. The simulation results verify the feasibility of the control method, but the dynamic model does not consider the nonlinear factors such as the dynamic friction of the system. In order to accurately describe the deployment process of the antenna, Xing [12] et al. used different dynamic modeling methods for different stages, including the deployable manipulator and the reflector. In addition, an attitude control method that does not depend on system parameter changes is proposed, in which the optimization method is adopted to achieve better anti-disturbance performance and enhance the robustness of the system. In order to form a complete controller baseline by advanced control theory, at the end of the ETS-VIII satellite mission, Nagashio [13] et al. conducted an on-orbit test of the spacecraft carrying two sets of deployable antennas to test the system's indicators such as resisting disturbance, robustness and stability. These control methods all rely on the dynamics model of the system. For nonlinear systems such as deployable antennas that are difficult to model accurately, the practicality of these methods is greatly reduced. For the time being, the research on control methods of antenna deployment process is insufficiency and imperfect, and this paper will propose different control strategies based on the accuracy of the dynamic model.

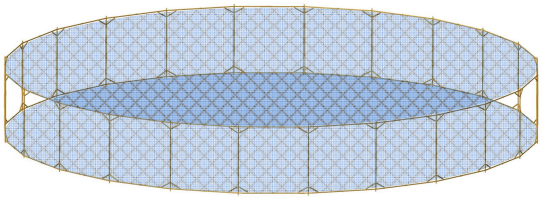

Fig. 2 A large space deployable antenna

In this paper, a new type of LDR developed by the team is introduced firstly. Based on the Lagrange method, the multi-body system dynamics model including rigid truss, flexible cable net and drive rope is built and analyzed briefly in Section II. Then two kinds of controllers—Backstepping controller and fuzzy PID controller are designed in Section III, where the former based on the dynamics model and the other not. In Section IV, the simulations of controllers are carried out, and the performance of each controller was compared and analyzed, and its feasibility was verified. The last section is a summary of this paper.

II. Mathematical Model of LDR

A. Structure Overview

The antenna truss studied in this paper is a high folding ratio ring deployable antenna consisting of 24 basic modules with characteristics of large diameter, low weight, and high capacity, and its deployment process is shown as Fig. 3. The structure of a single module is shown in Fig. 4. It is a closed combination of six-bar mechanism, adjacent modules are connected by a common crank slider. The motor drives the crank slider to move to both ends of the rod by pulling the rope, thereby deploying the entire annular truss mechanism. Under the constraint of two synchronous driving ropes, all variables can be represented by the deployable angle α.

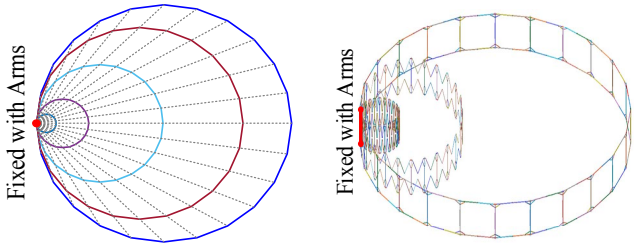

(a) Schematic diagram of the contour deployment process

(b) Schematic diagram of 3D deployment process

Fig. 3 LDR deployment diagram

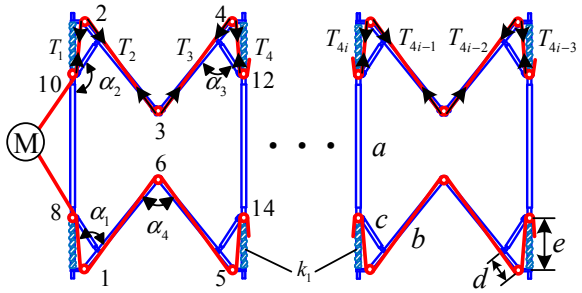

Fig. 4 Schematic diagram of basic module and driving system. Where a, b, c and d represent the length of each rod, and e represents the distance from the slider to the end of the rod.

B. Dynamic modeling

Since the author has established the dynamics model of the reflector system in detail in the literature [14], the key parts of the system mathematical model are briefly introduced here.

According to its deployable principle, the Lagrange dynamic equation (1) of the system including rigid truss, flexible cable net and driving rope is established,

$$\frac{d}{dt}\left(\frac{\partial(E-U)}{\partial\dot{\alpha}}\right)-\frac{d}{d\alpha}(E-U)=Q_F \tag{1}$$

where E, U and Q_F represent the kinetic energy, the potential energy and the generalized external force of the system respectively, $\dot{\alpha}$ represent the angular velocity of the deployment.

System kinetic energy E is the sum of kinetic energy of all modules and can be expressed as

$$E=\sum_{i=1}^{n}\left(\sum_{b=1}^{10}E_b+\sum_{j=1}^{14}E_j\right)=\frac{1}{2}J_\alpha\dot{\alpha}^2 \tag{2}$$

where E_b denotes the kinetic energy of each member and E_j denotes the kinetic energy of each joint, J_α represents the system equivalent moment of inertia, $\dot{\alpha}$ represents the generalized deployable velocity, and other kinetic energy is ignored.

The potential energy U is mainly derived from the tension of the cable net and spring k_1. The cable net is equivalent to a rigid net connected to the truss by spring k_2, so its potential energy can be expressed as

$$U=\begin{cases} nk_1\left(l_0-e\right)^2, & 0\le\alpha<\alpha_c \\ nk_1\left(l_0-e\right)^2+\dfrac{nk_2b^2(\sin\alpha-\sin\alpha_c)^2}{\sin^2(180°/n)}, & \alpha\ge\alpha_c \end{cases} \tag{3}$$

where α_c represents the critical angle of the cable tension, l_0 represents the natural length of the spring. When the deployment angle α is lower than α_c, only the potential energy of the compression spring is increasing. When the deployment angle α is higher than α_c, the potential energy of the compression spring and the cable net system are rising.

The system generalized force Q_F consists of the joint friction Q_f and the tension Q_T of the driving rope, which can be expressed as,

$$\begin{aligned} Q_F &= Q_f+Q_T \\ &= -n\xi_1\sum_{i=1}^{14}\dot{\alpha}_i\frac{\partial\alpha_i}{\partial\alpha}-2n\xi_2\dot{e}\frac{\partial e}{\partial\alpha}+2\sum_{i=1}^{n}\left(Q_{T_{4i-3}}+Q_{T_{4i-2}}+Q_{T_{4i-1}}+Q_{T_{4i}}\right) \\ &= -n\xi_1\sum_{i=1}^{14}\dot{\alpha}_i\frac{\partial\alpha_i}{\partial\alpha}-2n\xi_2\dot{e}\frac{\partial e}{\partial\alpha}-2T_1\frac{\partial e}{\partial\alpha}\sum_{i=1}^{n}\left[e^{-4\mu(i-1)(\pi-\alpha)}\left(1+e^{-\mu(3\pi-4\alpha)}\right)\right] \end{aligned} \tag{4}$$

where ξ_1 and ξ_2 represents the friction coefficient of the rotating joint and the moving joint, μ represents the friction coefficient of the pulley surface, T_1 represents the force of the motor acting on each drive rope.

Bring (2), (3) and (4) established above into the Lagrange equation (1) and simplify,

$$J_\alpha\ddot{\alpha}+\frac{1}{2}\frac{\partial J_\alpha}{\partial\alpha}\dot{\alpha}^2+Q_f+\frac{\partial U}{\partial\alpha}-Q_T=0 \tag{5}$$

Equation (5) is the dynamic model of the antenna, a second-order nonlinear time-varying system.

C. State space equation representation

According to modern control theory, the antenna system dynamics model is described by state space equations. Suppose the system input is u, let $\chi_1=\alpha$, $\chi_2=\dot{\alpha}$, $\dot{\chi}_1=\dot{\alpha}$, $\dot{\chi}_2=\ddot{\alpha}$, so the original dynamic equation can be expressed as,

$$\begin{cases} \dot{\chi}_1=\chi_2 \\ \dot{\chi}_2=f(\chi_1,\chi_2)+g(\chi_1)u \end{cases} \tag{6}$$

where

$$\begin{cases} f(\chi_1,\chi_2)=-\dfrac{1}{J_\alpha}\left(\dfrac{1}{2}\dfrac{dJ_\alpha}{d\chi_1}\chi_2^2+\xi\chi_2+\dfrac{dU}{d\chi_1}\right) \\ g(\chi_1)=2J_\alpha^{-1}\dfrac{\partial e}{\partial\alpha}\sum_{i=1}^{n}\left[e^{-4\mu(i-1)(\pi-\alpha)}\left(1+e^{-\mu(3\pi-4\alpha)}\right)\right] \end{cases} \tag{7}$$

According to equation (7), $g(\chi_1)>0$, it is known that $g^{-1}(\chi_1)$ exists.

III. Control System Design

Although the dynamics model is established in section II, the established dynamic model is not very accurate due to inevitable manufacturing errors and assembly accuracy and some nonlinear factors such as temperature changes in outer space. The Backstepping controller and fuzzy PID controller are designed respectively based on the model and non-model respectively in this section.

A. Backstepping controller design

The Backstepping-based control method belongs to a recursive design method, which is simple in thought, easy to understand, and has important applications in practical engineering.

Step 1, according to the system dynamics model described in (6), the actual output of the system is χ_1, assuming that the expected system output is assumed to be χ_{1d}, and the error of the first subsystem is defined as

$$\begin{cases} \delta_1=\chi_{1d}-\chi_1 \\ \dot{\delta}_1=\dot{\chi}_{1d}-\dot{\chi}_1=\dot{\chi}_{1d}-\chi_2 \end{cases} \tag{8}$$

Define a Lyapunov function,

$$\begin{cases} V_1(\delta_1)=\dfrac{1}{2}\delta_1^2 \\ \dot{V}_1(\delta_1)=\delta_1\dot{\delta}_1=\delta_1(\dot{\chi}_{1d}-\chi_2) \end{cases} \tag{9}$$

According to the Lyapunov direct method, in order to make δ_1 close to 0, $\dot{V}_1(\delta_1)$ is always guaranteed to be a negative definite function. Therefore

$$\chi_{2d}=\dot{\chi}_{1d}+K_1\delta_1 \tag{10}$$

where K_1 is a positive gain coefficient.

Step 2, define the error of the second subsystem as

$$\begin{cases} \delta_2=\chi_{2d}-\chi_2 \\ \dot{\delta}_2=\dot{\chi}_{2d}-\dot{\chi}_2=\ddot{\chi}_{1d}+K_1\dot{\delta}_1-f(\chi_1,\chi_2)-g(\chi_1)u \end{cases} \tag{11}$$

Similarly, in order to make χ_2 approach χ_{2d}, both δ_1 and δ_2 need to be close to 0, so the second Lyapunov function is defined as,

$$\begin{cases} V_2(\delta_1,\delta_2)=\dfrac{1}{2}\delta_1^2+\dfrac{1}{2}\delta_2^2 \\ \dot{V}_2(\delta_1,\delta_2)=-K_1\delta_1^2+\delta_1\delta_2+\delta_2\dot{\delta}_2=-K_1\delta_1^2+\delta_2\left(\delta_1+\dot{\delta}_2\right) \end{cases} \tag{12}$$

In order to make $\dot{V}_2(\delta_1,\delta_2)$ a negative definite function, define

$$\delta_1+\dot{\delta}_2=-K_2\delta_2 \tag{13}$$

where K_2 is a positive gain coefficient. According to equation (11) and (13), the control law u can be obtained,

$$u=\frac{1}{g(\chi_1)}\left[\chi_{1d}-\chi_1+\ddot{\chi}_{1d}+K_1\dot{\delta}_1+K_2\delta_2-f(\chi_1,\chi_2)\right] \tag{14}$$

Through the control law, the system satisfies the Lyapunov stability condition, thus ensuring the global asymptotic stability of the system.

B. Self-tuning fuzzy-PID controller design

The parameters of the classical PID control (proportional, integral, differential) are constant values obtained according to the precise mathematical model, which cannot be adaptively adjusted online according to external disturbances and system parameter changes. The fuzzy logic system is an inference system that simulates human brain thinking, which does not depend on an accurate system model, and can adjust the output according to the changes of system parameters. Fuzzy PID (FPID) controller, combining PID with fuzzy control, is not only easy to implement, but also adaptive to system changes to adjust PID parameters. This method is very suitable for

complex nonlinearities time-varying systems such as antennas that are difficult to accurately model.

The principle of fuzzy-PID control can be expressed as

$$u(t)=K_p e(t)+K_i\int_0^t e(t)dt+K_d\frac{d}{dt}e(t) \tag{15}$$

where $e(t)$ represents the difference between the system input $r(t)$ and output $\chi(t)$ at the current sampling time, K_p, K_i, and K_d are proportional, integral, and differential gain coefficients, respectively, which are expressed as

$$\begin{cases} K_p = K_{p0}+\mu_p\Delta K_p \\ K_i = K_{i0}+\mu_i\Delta K_i \\ K_d = K_{d0}+\mu_d\Delta K_d \end{cases} \tag{16}$$

where K_{p0}, K_{i0}, and K_{d0} represent the initial values, ΔK_p, ΔK_i, and ΔK_d represent the parameter adjustment values obtained after the fuzzy logic, and μ_p, μ_i, and μ_d respectively represent the quantized coefficients of the respective parameters, selected according to the range of parameter values. The diagram of the FPID controller is shown in Fig. 5.

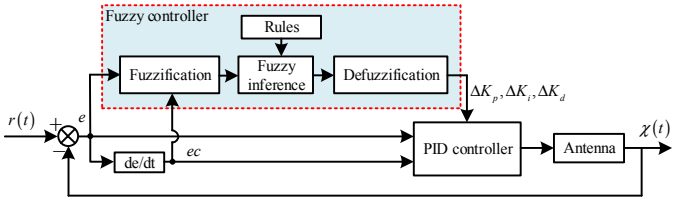

Fig. 5 Schematic diagram of the FPID controller

The fuzzy controller adopts the two-input and three-output two-dimensional fuzzy structure of the Mamdani model. The core is to use the difference $e(t)$ of the input trajectory and the output trajectory and its rate of change $ec(t)$, after fuzzification, fuzzy reasoning and defuzzification to adjust the three parameters adaptively.

Specifically, first, two input variables need to be blurred, and each input variable corresponds to seven fuzzy sets, which are {NB, NM, NS, ZE, PS, PM, PB}. The membership function of different shapes has a great influence on the control performance of the system. The strategy adopted in this paper is to select the low-resolution membership function for larger errors and the high-resolution for smaller errors. The membership function needs to take into account the computational complexity, so the seven fuzzy sets use the triangle membership function, as shown in the input of Fig. 6.

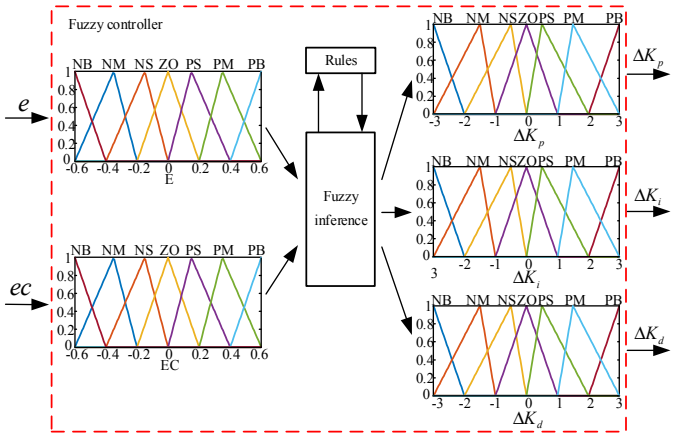

Fig. 6 Structure of Mamdani fuzzy controller

Secondly, the FPID controller uses the "IF-THEN" rule according to the rule base to generate the adjusted fuzzy values of the three parameters controlled by the PID. Since the input values E and EC each contain seven fuzzy subsets, a total of 49 fuzzy rules are generated, and the i-th rule can be expressed as

R^i: If $E=\Phi_1$ and $EC=\Phi_2$

Then $\Delta K_p=\Phi_3$, $\Delta K_i=\Phi_4$, $\Delta K_d=\Phi_5$

where Φ_i represents a fuzzy set of individual variables. The fuzzy rule base is based on expert experience and engineering practice experience, which is shown in Table I.

TABLE I
FUZZY-PID RULE BASE

$\Delta K_p \mid \Delta K_i \mid \Delta K_d$		E						
		NB	NM	NS	ZO	PS	PM	PB
EC	NB	PB/NB/PS	PB/NB/PS	PB/NB/ZO	PM/NM/ZO	PS/NM/ZO	PS/ZO/PM	ZO/ZO/PB
	NM	PB/NB/PS	PB/NB/NS	PM/NM/NS	PM/NM/NS	PS/NS/ZO	ZO/ZO/PM	ZO/ZO/PM
	NS	PM/NM/NB	PM/NM/NM	PM/NS/NS	PS/NS/ZO	ZO/ZO/PS	NS/PS/PM	NM/PS/PM
	ZO	PM/NM/NM	PS/NS/NM	PS/ZO/NS	PS/PS/ZO	NS/PS/PM	NM/PS/PM	NM/PM/PM
	PS	PS/NS/NB	PS/NS/NM	ZO/ZO/NS	NS/PS/NS	NS/PS/ZO	NM/PM/PS	NM/PM/PS
	PM	ZO/ZO/NM	ZO/ZO/NS	NS/PM/NS	NM/PM/NS	NM/PM/ZO	NM/PB/PS	NB/PB/PS
	PB	ZO/ZO/PS	NS/PS/PS	NS/PM/PS	NM/PM/PM	NM/PB/PM	NB/PB/PB	NB/PB/PB

The value obtained after fuzzy inference is the fuzzy value of the variable, which needs to be defuzzified to obtain the value of the control variable that can be accepted by the controlled object. The output variables ΔK_p, ΔK_i, and ΔK_d are also divided into seven fuzzy subsets respectively, and the triangular membership functions with sparse edges on both sides are used, as shown in the output of Fig. 6. The output values are then quantized according to the scale to obtain a suitable output value. The FPID can adjust the proportional gain, the integral gain and the differential gain in real-time according to system parameter changes and external disturbances, thereby greatly improving the performance of the system.

IV. NUMERICAL SIMULATION AND RESULTS

This section simulates the two controllers presented above. The initial deployment angle α of the folded state of the LDR

is α_0, and the angle α is $\pi/2$ after the full deployment. The ideal deployable trajectory of the antenna system is a Bezier curve obtained by the principle of minimizing the acceleration,

$$\alpha(t)=\sum_{i=0}^{m}\left(\alpha_i\cdot\frac{m!}{i!(m-i)!}t^i(1-t)^{m-i}\right),\ t\in[0,1] \qquad (17)$$

where t represents the quantization time, α_i is control points of the Bezier curve, which can be obtained by an optimization algorithm for seeking the smallest deploying acceleration peak value, $\alpha_i|_{i=0\sim m}$ = (0.0768, 0.0768, 0.0768, 0.4465, 0.8152, 1.2169, 1.5708, 1.5708, 1.5708), m is the number of control points. In addition, the parameter information of the LDR system is shown in Table II.

TABLE II
SYSTEM PARAMETERS

Parameters	Values	Parameters	Values
a	1 m	α_c	80°
b	0.45 m	k_1	100 N/m
c	0.1 m	k_2	200 N/m
d	0.15 m	l_0	0.3 m
n	24	ξ_1	0.1
ρ	1800 kg/m^3	ξ_2	0.1
α_0.	4.4°	μ	0.01

A. *Backstepping controller simulation*

Two scenarios are considered when simulating the Backstepping controller. One is ideally, that is, the simulation of the system without external disturbances, and the other is the simulation of the system when there is a certain external disturbance $0.001\sin(0.2t)$. Both the controller module and the controlled object model are written using the S function, and the control law designed by (14) is adopted, in which the parameters are designed as $C_1=10$, $C_2=10$. The system simulation results are shown in Fig. 7 and Fig. 8.

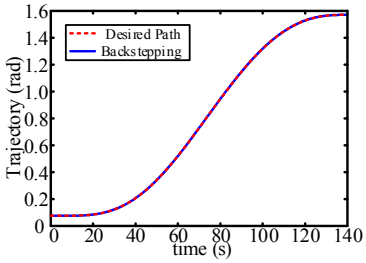

Fig. 7 Deployment path based on the backstepping controller

According to Fig. 7, it can be seen that under the action of the Backstepping controller, the LDR can track the planned Bezier trajectory very well. When there is no external disturbance, the error is difficult to observe, which shows the high accuracy of the control method. It can be seen from Fig. 8 that after obtaining the accurate model of LDR, the Backstepping-based controller has a small error on the trajectory tracking, reaching the order of 10^{-4} rad, even in the case of external disturbances. The output force of the controller can compensate for the external disturbance in time, which shows that the controller based on Backstepping has certain robustness and adaptability. However, according to the control equation (14), it is difficult to design an effective control law when the modeling information of the system is not perfect or the accurate model of the system cannot be obtained, which limits the use of the controller.

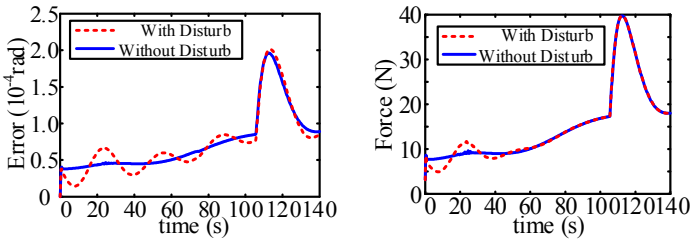

(a) Trajectory error (b) Control force

Fig. 8 Anti-disturbance performances of the Backstepping controller

B. *FPID controller simulation*

Firstly, the field of the input E and EC of the fuzzy PID controller are set to [-0.6, 0.6], the quantization parameter is defined as $180/\pi$, and the domain of the gain coefficient output by the controller is set to [-3, 3]. The initial values of gain, integral gain and differential gain are taken as $K_{p0}=160$, $K_{i0}=0.6$, $K_{d0}=20$, and the corresponding quantization parameters are $\mu_p=20$, $\mu_i=0.2$, $\mu_d=2$, respectively.

Secondly, in order to compare the performance of FPID and classic PID, the gain coefficients of the classic PID are set as the initial value of the FPID. In order to observe the dynamic response of the two controllers, an external shock disturbance is applied to the controlled object at the 30th second with an amplitude of 0.001. A simulation model as shown in Fig. 9 is established according to the principle of the controller, and results are shown in Fig. 10.

As shown in Fig. 10 (a), in the case where the system dynamics model cannot be established, the FPID controller can still accurately track the ideal trajectory. The FPID controller can produce smaller errors as shown by the classic PID shown in Fig. 10 (b). In the 30th second, where the system is subject to external interference, both the FPID and the classic PID controller respond to this, but the dynamic response time is also significantly lower than the classic PID control, which reflects the better response performance of the FPID. According to Fig. 10 (c) and Fig. 10 (d), since the fuzzy PID controller does not depend on the system dynamics model, it responds in real-time according to the error and its rate of change, so in the 104th second (the antenna cable network system begins), there will be a significant decrease in the speed of the system deployment, but then the controller responds in time, increasing the control of the system and ensuring that the system can be deployed according to a predetermined trajectory. Through simulation, it can be found that compared with the classical PID controller, by adaptively adjusting the gain coefficient of the PID, the trajectory tracking error and dynamic response performance generated by FPID controller are better, showing better interference immunity and robustness.

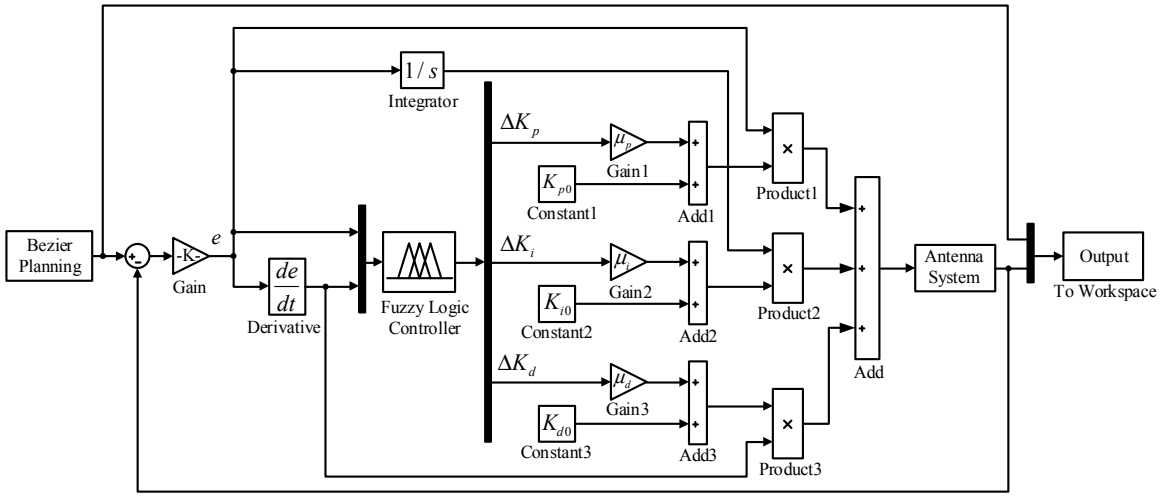

Fig. 9 Simulation model of FPID

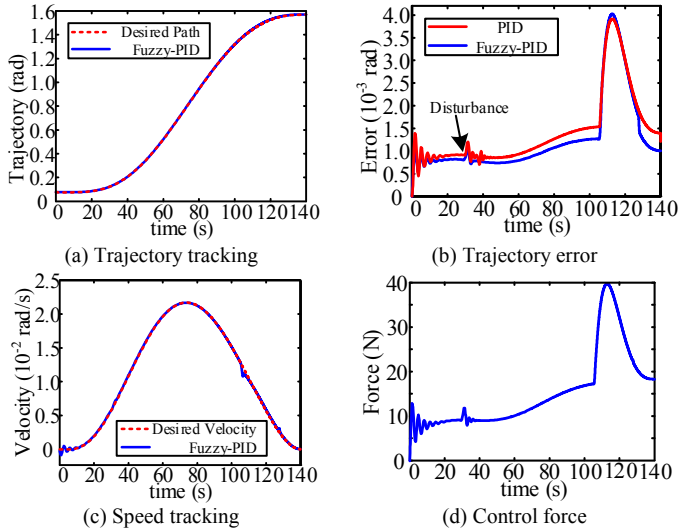

(a) Trajectory tracking (b) Trajectory error

(c) Speed tracking (d) Control force

Fig. 10 Simulation results of Fuzzy PID controller

V. Conclusion

This paper focuses on the deployment controller of a large space deployable antenna. At the beginning of the paper, the antenna structure and dynamic model of the antenna is described, and the state space equation is established based on modern control theory. The deployment controller is based on two different situations. Firstly, assuming that the dynamic model parameters of the system are known and the dynamic equations are accurate, a Backstepping-based controller is designed, and a control law that relies on an accurate model is proposed. Secondly, independent of the system model, a controller is designed with fuzzy PID. The difference between the input and output adjusts the parameters of the PID controller in real-time to enhance the dynamic response performance of the system. According to the simulation results, the Backstepping controller exhibits good tracking performance and robust performance with accurate dynamics model; the fuzzy PID controller continuously adjusts the parameters during the antenna deployment process, showing superior performance over PID. The research results of this article can be used in the future deployment control of such antennas.

References

[1] Y. Rahmat-Samii, and A. C. Densmore, "Technology trends and challenges of antennas for satellite communication systems," IEEE Trans. Antennas Propag., vol. 63, no. 4, pp. 1191-1204, 2015.

[2] M. Mobrem, S. Kuehn, C. Spier, and E. Slimko, "Design and performance of astromesh reflector onboard soil moisture active passive spacecraft," in IEEE Aerosp. Conf., March 2012 pp. 1-10.

[3] M. Tafazoli, "A study of on-orbit spacecraft failures," Acta Astronaut., vol. 64, no, 2-3, pp. 195-205, 2009.

[4] H. Tanaka, and R. Sakamoto, "Effects of vibration characteristics on improvement of deployment repeatability by vibration," Aerosp. Sci. Technol., vol. 84, pp. 839-844, 2019.

[5] C. Shi, H. Guo, M. Li, R. Liu, and Z. Deng, "Conceptual configuration synthesis of line-foldable type quadrangular prismatic deployable unit based on graph theory," Mech. Mach. Theory, vol. 121, pp. 563-582, 2018.

[6] H. Guo, X. Song, L. Li, Z. Deng, R. Liu, and J. Geng, "Type synthesis of deployable single-loop overconstrained linkages based on Bennett linkages," Mech. Mach. Theory, vol. 120, pp. 1-29, 2018.

[7] X. Qi, H. Huang, Z. Miao, B. Li, and Z. Deng, "Design and mobility analysis of large deployable mechanisms based on plane-symmetric Bricard linkage," J. Mech. Des., vol. 139, no. 2, p. 022302, 2017.

[8] B. Li, X. Qi, H. Huang, and W. Xu, "Modeling and analysis of deployment dynamics for a novel ring mechanism," Acta Astronaut., vol. 120, pp. 59-74, 2016.

[9] X. Qi, H. Huang, B. Li, and Z. Deng, "A large ring deployable mechanism for space satellite antenna," Aerosp. Sci. Technol., vol. 58, pp. 498-510, 2016.

[10] Y. Zhang, B. Duan, and T. Li, "A controlled deployment method for flexible deployable space antennas," Acta Astronaut., vol. 81, no. 1, pp. 19-29, 2012.

[11] Y. Zhang, D. Yan, and S. Li, "An integrated control and structural design approach for mesh reflector deployable space antennas," Mechatron., vol. 35, pp. 71-81, 2016.

[12] Z. Xing, and G. Zheng, "Deploying process modeling and attitude control of a satellite with a large deployable antenna," Chin. J. Aeronaut., vol. 27, no. 2, pp. 299-312, 2014.

[13] T. Nagashio, T. Kida, T. Ohtani, and Y. Hamada, "Design and implementation of robust symmetric attitude controller for ETS-VIII spacecraft," Control Eng. Pract., vol. 18, no. 12, pp. 1440-1451, 2010.

[14] S. Lu, X. Qi, Y. Hu, B. Li, and J. Zhang, "Deployment Dynamics of Large Space Antenna and Supporting Arms," IEEE Access, vol. 7, pp. 69922-69935, 2019.